JACS
JOURNAL OF THE AMERICAN CHEMICAL SOCIETY
Article
pubs.acs.org/JACS

Combined Charge Carrier Transport and Photoelectrochemical Characterization of $BiVO_4$ Single Crystals: Intrinsic Behavior of a Complex Metal Oxide

Alexander J. E. Rettie,[†] Heung Chan Lee,[‡] Luke G. Marshall,[§] Jung-Fu Lin,[∥] Cigdem Capan,[⊥] Jeffrey Lindemuth,[@] John S. McCloy,[#] Jianshi Zhou,[§] Allen J. Bard,[‡] and C. Buddie Mullins*[,†,‡,§]

[†]McKetta Department of Chemical Engineering, The University of Texas at Austin, Austin, Texas 78712, United States

[‡]Center for Electrochemistry, Department of Chemistry and Biochemistry, The University of Texas at Austin, Austin, Texas 78712, United States

[§]Materials Science and Engineering Program, Texas Materials Institute, Department of Mechanical Engineering, The University of Texas at Austin, Austin, Texas 78712, United States

[∥]Department of Geological Sciences, The University of Texas at Austin, Austin, Texas 78712, United States

[⊥]Department of Physics and Astronomy, Washington State University, Pullman, Washington 99164, United States

[@]Lake Shore Cryotronics, Westerville, Ohio 43081, United States

[#]Energy and Environment Directorate, Pacific Northwest National Laboratory, Richland, Washington 99354, United States

Supporting Information

ABSTRACT: Bismuth vanadate ($BiVO_4$) is a promising photoelectrode material for the oxidation of water, but fundamental studies of this material are lacking. To address this, we report electrical and photoelectrochemical (PEC) properties of $BiVO_4$ single crystals (undoped, 0.6% Mo, and 0.3% W:$BiVO_4$) grown using the floating zone technique. We demonstrate that a small polaron hopping conduction mechanism dominates from 250 to 400 K, undergoing a transition to a variable-range hopping mechanism at lower temperatures. An anisotropy ratio of ∼3 was observed along the *c* axis, attributed to the layered structure of $BiVO_4$. Measurements of the ac field Hall effect yielded an electron mobility of ∼0.2 $cm^2 V^{-1} s^{-1}$ for Mo and W:$BiVO_4$ at 300 K. By application of the Gärtner model, a hole diffusion length of ∼100 nm was estimated. As a result of low carrier mobility, attempts to measure the dc Hall effect were unsuccessful. Analyses of the Raman spectra showed that Mo and W substituted for V and acted as donor impurities. Mott−Schottky analysis of electrodes with the (001) face exposed yielded a flat band potential of 0.03−0.08 V versus the reversible H_2 electrode, while incident photon conversion efficiency tests showed that the dark coloration of the doped single crystals did not result in additional photocurrent. Comparison of these intrinsic properties to those of other metal oxides for PEC applications gives valuable insight into this material as a photoanode.

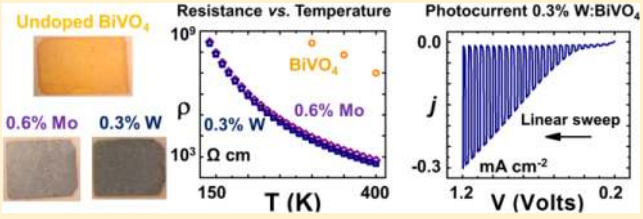

1. INTRODUCTION

Photoelectrochemical (PEC) water splitting has great potential as a route to renewable hydrogen production using solar energy.[1,2] However, a lack of efficient, inexpensive, and stable photoelectrodes inhibits this technology. Metal oxides are promising candidate materials because of their stability and relative abundance but often have poor light absorption and charge transport properties. Pertinent examples of metal oxide photoelectrode materials include titania (TiO_2),[3] hematite (α-Fe_2O_3),[4] and tungsten oxide (WO_3).[5] In the continuing search for higher efficiencies, complex metal oxides, with two or more cations, are coming to the forefront of this field.

Monoclinic bismuth vanadate ($BiVO_4$) is one such promising material for water oxidation.[6−8] It is attractive because of its direct band gap of ∼2.4 eV, favorably positioned band edges, and stability when coupled with cocatalysts. The monoclinic structure ("clinobisvanite") is the most common under ambient conditions and has also been shown to be the most photocatalytically active.[9] The crystal is a slightly distorted tetragonal scheelite structure, which converts to an undistorted scheelite structure with temperature,[10] pressure,[11] or the addition of dopants.[12] Recently, polycrystalline $BiVO_4$ photoelectrodes singly doped with molybdenum (Mo)[13−16] or tungsten (W)[15,17−19] or codoped with Mo and W[20,21] have led to increased efficiencies and thus motivated us to perform a fundamental study of the electrical properties of this system using well-characterized single crystals.

In 1979, Sleight et al. first made synthetic single crystals of $BiVO_4$ using the Czochralski technique.[22] Additionally, Hoffart

Received: June 3, 2013
Published: July 8, 2013

   dx.doi.org/10.1021/ja405550k | J. Am. Chem. Soc. 2013, 135, 11389−11396

et al. measured the conductivity of $BiVO_4$ single crystals at high temperatures (550−700 °C) where the tetragonal scheelite phase is dominant and conduction is primarily ionic.[23] Several investigations of conduction in polycrystalline samples have been performed,[24−28] but variation in syntheses and grain boundary effects limit the general application of these results. Determinations of carrier properties, such as mobility and diffusion length, are inherently difficult, as most metal oxides are highly electrically resistive at temperatures applicable to PEC cell operation (room temperature to 100 °C for aqueous electrolytes).

The aim of this study was to measure the intrinsic electrical properties of $BiVO_4$. To the best of our knowledge, this is the first report of doped $BiVO_4$ single crystals. Once these crystals were obtained, they were oriented and either characterized electrically or used as photoelectrodes. The term "doping" will be used in this paper to describe the addition of impurities to change a material's electrical properties, without the formation of secondary phases.

The crystal phase and composition were studied using X-ray diffraction, inductively coupled plasma mass spectrometry, and Raman spectroscopy. Electrical properties were obtained by measuring the resistivity and the Hall effect as functions of temperature. Oriented samples were used to probe potential anisotropy. Finally, PEC tests under illumination, Mott-Schottky analysis and estimation of the hole diffusion length were performed.

2. EXPERIMENTAL METHODS

2.1. Single-Crystal Synthesis. Starting ceramic powders were made by a solid state reaction of Bi_2O_3 (99.999%, Sigma-Aldrich), V_2O_5 (99.6%, Sigma-Aldrich), MoO_3 (99.95%, Alfa Aesar), and WO_3 (99.99%, K. J. Lesker). After being mixed in an agate mortar, these mixtures were calcined first at 600 °C for 10 h before further reaction at 900 °C for 10 h in air with intermediate mixing. Mo and W were added on the basis of the chemical formula

$$Bi_{1-x/3}Ø_{x/3}V_{1-x}M_xO_4 \quad (1)$$

where Ø represents Bi vacancies and M is Mo or W.[12,29]

Single crystals were grown using an infrared heating image furnace (NEC SC-M35HD). The ceramic powders were isostatically pressed to form the feed and seed rods before a final annealing step of 700 °C for 10 h. A slight excess of V (48:52 Bi:V atom % ratio) was added to these powders to account for volatilization losses.[23] The feed and seed rods were counter-rotated at 30 rpm in a static O_2 atmosphere of 1.8 atm during the growth. Typical growth rates were between 1 and 3 mm/h. In some cases, the feed rods were premelted prior to growth to suppress bubble formation in the melt zone.

2.2. Composition. Powder X-ray diffraction (XRD) was performed using a Philips X'Pert diffractometer equipped with monochromatic Cu Kα X-rays (λ = 1.54056 Å). Laue back-reflection XRD was employed to check single-crystal quality and to orient crystals in the three principal crystallographic axes to within 1°. Multiple Laue images were taken on samples to ensure they were single-domain throughout. Inductively coupled plasma mass spectrometry (ICP-MS) measurements were taken using an Agilent 7500ce Quadrupole ICP-MS instrument. To prepare samples for ICP-MS, powders from the single crystals were dissolved in 4 M HNO_3 (Fisher) and reacted at 180 °C for 2 h in a Teflon-lined autoclave (Parr). Deionized water was used throughout the ICP-MS sample preparation. An optical Raman system with a Verdi V2 532 nm green laser, Andor spectrometer, iCCD detector, and 1800 grating was utilized for vibrational spectroscopy measurements. Diffuse reflectance UV−vis spectra were measured with a Cary 500 spectrophotometer attached to an integrating sphere (Labsphere DRA-CA-5500).

2.3. Electrical Measurements. The dc resistivity and dc field Hall effect measurements were taken using a Physical Property Measurement System (PPMS, Quantum Design) specially modified for high-resistivity samples at Pacific Northwest National Laboratory.[30] A custom sample probe with triax connectors was used for this work. The ac field Hall effect measurements were taken at Lake Shore Cryotronics on a model 8404 ac/dc Hall measurement system. Some resistivity measurements at room temperature were taken using a Keithley 2400 source meter.

The sample geometry was rectangular, oriented such that measurements could be made along principal crystallographic axes [Figure S1 of the Supporting Information (SI)]. It was not practical to differentiate between the *a* and *b* axes using Laue XRD because of the near structural symmetry in these directions; therefore, they were combined and termed *ab*. The thicknesses of the single crystals ranged from 160 to 220 μm.

Ohmic contact was achieved by using In−Ga eutectic (Sigma-Aldrich), held in place with Ag paste (CircuitWorks). When indium metal or only Ag paste was used, high resistances and diode behavior were observed (Figure S2 of the SI). Contact areas at the edges were kept small (~0.1 mm^2) to minimize measurement errors. Current−voltage curves taken at all chosen temperatures confirmed that the contacts were ohmic (Figure S3 of the SI).

The dc resistivity was measured from 400 to 140 K in the van der Pauw (vdP) configuration. The dc field Hall effect data were obtained with a magnetic field of −6 to 6 T applied perpendicular to the sample. The dc current was applied in both polarities at each field and temperature to eliminate intrinsic errors resulting from misaligned contacts.[31] Experimental errors commonly found in high-resistivity samples due to sample capacitance and temperature transients were minimized by waiting for the current and voltage signal to reach the steady state after the temperature, field, or current had been changed. The ac field Hall effect data were obtained with a magnetic field frequency of 0.1 Hz. This frequency is large enough such that ac conductivity effects can be ignored (further explanation in the SI). The dc current was applied in both polarities to remove the inductive pickup signal from the Hall voltage.[32]

2.4. Photoelectrochemical Measurements. Single crystals were incorporated in electrodes using an In−Ga eutectic/Ag paste back-contact embedded in nonconductive epoxy (Loctite). A freshly cleaved (001) face was exposed, and electrode areas were between 1 and 2 mm^2. The crystal thicknesses ranged from 80 to 150 μm.

Photoelectrochemical measurements were conducted in a three-electrode cell using the single crystal as the working electrode, Ag/AgCl (saturated KCl) as the reference electrode, and Pt wire as the counter electrode. All potentials reported here are versus the reversible H_2 electrode (RHE). Illumination was the full output of a 150 W Xe lamp (Osram, Munich, Germany) calibrated to 100 mW/cm^2. A monochromator (Photon Technology International), a silicon photodetector (model 818-UV, Newport), and an optical power meter (model 1830-C, Newport) were used to obtain the incident photon to current conversion efficiency (IPCE). IPCE values were calculated using the formula[33]

$$\mathrm{IPCE}(\lambda) = \frac{1240j(\lambda)}{\lambda E(\lambda)} \times 100 \quad (2)$$

where λ is the wavelength (nanometers), j is the photocurrent density, and E is the incident power of the monochromated light.

The electrolyte solution was 0.1 M phosphate buffer with 0.1 M Na_2SO_4 (Fisher) in deionized Milli-Q water (pH 7). In some experiments, 0.1 M Na_2SO_3 (Fisher) was added to this solution as a hole scavenger (pH 7). A CH Instruments 630D potentiostat was used for all current−voltage scans. The scan rate was 20 mV/s. Capacitance−voltage measurements were taken using a CH Instruments 660D potientiostat. The amplitude of the applied voltage was 5 mV at fixed frequencies of 500, 1000, and 1500 Hz.

dx.doi.org/10.1021/ja405550k | J. Am. Chem. Soc. 2013, 135, 11389−11396

3. RESULTS AND DISCUSSION

3.1. Synthesis. Crystal boules of undoped and doped (<1 atom %) $BiVO_4$, ~6 mm in diameter and 20 mm in length, were prepared but were rarely single-domain throughout. This is in agreement with other studies, where $BiVO_4$ crystals grown by the Czochralski technique contained extensive twinning.[22,23] Regardless, large single crystals (up to 4 mm × 3 mm × 2 mm in our case) could be cut from the boules. Laue back-reflection XRD confirmed that the prepared samples were not macroscopically twinned (Figure S4 of the SI). The undoped crystals were transparent orange, and we saw cleavage perpendicular to the *c* axis as observed by other workers.[22,23] Figure 1 shows that

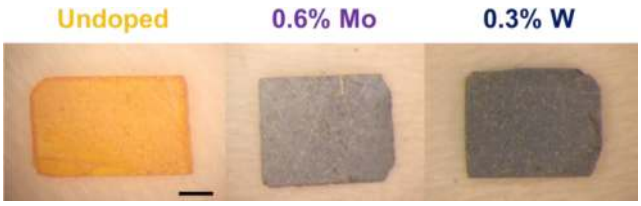

Figure 1. Photographs of undoped and doped oriented and polished single-crystal *c* plates. The scale bar is 1 mm.

doping with Mo and W changed the apparent color to a dark purple. Observed color can be due to a variety of mechanisms;[34] in this case, we rationalize the color change using semiconductor band theory. Mo and W are predicted to act as shallow donor impurities,[20,35] which gives rise to a low-energy transition between the impurity states and the conduction band, capable of absorbing all visible photons. Grinding of both doped and undoped crystals resulted in yellow powder characteristic of $BiVO_4$, indicating that the dark purple color is observed only in specimens where the crystal domains are large enough. This phenomenon is well-known in mineralogy, where "streak" (dragging a sample across a hard plate to produce a fine powder) is used to identify compounds.[36]

Higher doping concentrations, up to 10%, were attempted but resulted in an unstable melt zone, which was presumably caused by incongruent melting. Incongruently melting materials can be grown using the traveling solvent floating zone technique,[37] but the use of a suitable solvent is essential. Several solvents in the Bi_2O_3–V_2O_5 phase diagram were tried, but none resulted in stable crystal growth. More exotic solvent materials may be successful.

3.2. Compositional Analysis. Final dopant concentrations were determined by inductively coupled plasma mass spectrometry (ICP-MS), confirming that Mo and W were present in the samples. Results are shown in Table 1. From these values, it appears that *x* in eq 1 is limited to ~0.3% for W in $BiVO_4$ grown from the melt. In fact, the value of *x* decreased for all samples, except sample 1, where the increase in the Mo concentration is attributed to V evaporation during growth. Hereafter, all data in this paper refer to either undoped, 0.6% Mo doped, or 0.3% W doped $BiVO_4$ single crystals. The doped samples will be termed Mo:$BiVO_4$ and W:$BiVO_4$. In this analysis, we have assumed that the doping in the samples is homogeneous; i.e., no surface segregation takes place. As mentioned in section 3.1, the melt–growth technique produces large boules of crystalline material, from which samples are cut. As the samples are obtained from the bulk of the boules, surface segregation is unlikely.

Table 1. Initial Calculated Dopant Concentrations in the Feed Rods Compared to the Concentrations Determined by ICP-MS in $BiVO_4$ Single Crystals

dopant	sample	starting x^a (%)	final x^a (%)
Mo	1	0.54	0.57
	2	1.08	0.78
W	3	0.52	0.31
	4	1.04	0.31

[a] *x* is based on eq 1.

Analyses of the powder X-ray diffraction (XRD) spectra showed that the resulting crystals were single-phase monoclinic $BiVO_4$ (PDF 14-0688) as shown in Figure 2. The addition of

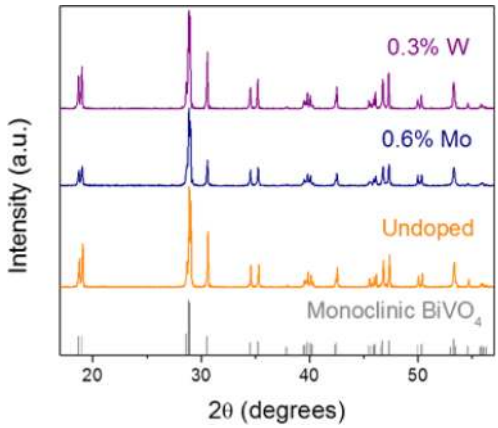

Figure 2. XRD patterns for pulverized $BiVO_4$ single crystals. Gray vertical ticks show the pattern for the monoclinic phase of $BiVO_4$ (PDF 14-0688).

Mo and W has been shown to stabilize the tetragonal scheelite structure of polycrystalline $BiVO_4$ at room temperature with high (>5 atom %) dopant concentrations.[12,20,21] The dopant concentrations that could be achieved using the floating zone growth process (<1%) were too small to yield any significant change in the lattice parameters, so the incorporation of Mo and W could not be studied using XRD.

Raman spectra were collected from the *c* plates of the single crystals to probe potential changes in the V site in the $BiVO_4$ lattice. All peaks could be indexed to Raman bands of monoclinic $BiVO_4$.[38,39] Luo et al. recently performed Raman spectroscopy on $BiVO_4$ thin films doped with 3 atom % Mo or W.[15] Doping resulted in little change between spectra, except for a shift of ~7 cm^{-1} in the peak around 829 cm^{-1} associated with stretching of the V–O bond. We measured a comparable shift of ~2 cm^{-1} in this peak, which we also assign to Mo and W substitution in the V site (Figure 3). Though the shift was small, it was repeatable. The low concentration of dopants made analyses of their charge state and local environment by X-ray photoelectron spectroscopy (XPS) impossible.

3.3. Electrical Transport. Resistivity was measured from 400 to 140 K, increasing by 5 orders of magnitude as the temperature was decreased (Figure 4). The similarity in the resistivity values for Mo and W doping was expected as their concentrations are comparable and both are typically in the +6 oxidation state,[20,21] therefore adding a single electron to the lattice per dopant atom. Undoped crystals were highly resistive (~5 × 10^8 Ω cm), compared with a value of ~10^4 Ω cm for

dx.doi.org/10.1021/ja405550k | J. Am. Chem. Soc. 2013, 135, 11389–11396

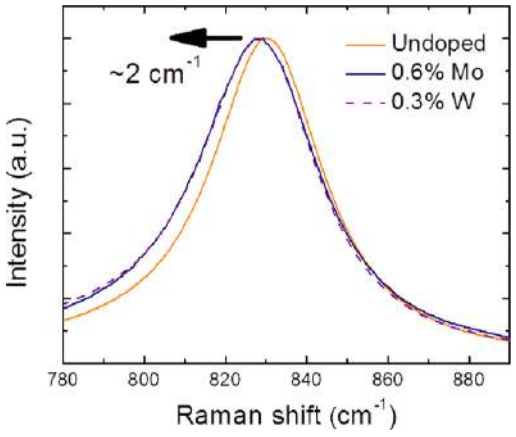

Figure 3. Raman spectra of single-crystal *c* plates, illustrating a shift in the peak around 830 cm^{-1}.

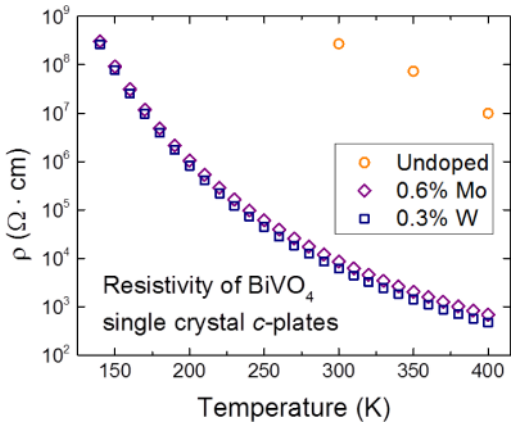

Figure 4. Resistivity vs temperature for $BiVO_4$ single crystals.

doped samples at 300 K. The van der Pauw (vdP) configuration was used, and there was little difference between the resistances along the *a* or *b* axis, indicating that $\rho_a \approx \rho_b$. Thus, *c* plates were assumed to be isotropic.

3.3.1. Transport Models. In many metal oxides (i.e., Ti:Fe_2O_3[40,41] and Nb:TiO_2[42]), carrier transport is described by a thermally activated small polaron hopping (SPH) mechanism first proposed by Mott.[43] In this model, the charge carrier distorts the surrounding lattice, impeding its transport and resulting in low mobility: an upper limit of 0.1−1 $cm^2\ V^{-1}\ s^{-1}$ has been calculated.[44] On the basis of density functional theory calculations,[20] SPH was suggested to be dominant in Mo:$BiVO_4$ and W:$BiVO_4$, with electron transport taking place between V^{4+} and V^{5+}, Mo^{6+}, or W^{6+} atoms. The small polaron model is described by[45]

$$\rho(T) \propto T \exp\left(\frac{E_a}{k_B T}\right) \tag{3}$$

where E_a is the hopping activation energy, k_B is Boltzmann's constant, and T is the absolute temperature. As shown in Figure 5, this model fits the data closely from 250 to 400 K, and activation energies of 0.286(1) and 0.290(1) eV were determined for Mo:$BiVO_4$ and W:$BiVO_4$, respectively. These results indicate that Mo and W have electrically similar behavior as dopants in the $BiVO_4$ system at concentrations of <1%.

A transition to a variable range hopping (VRH) mechanism is expected at low temperatures, at approximately one-half the

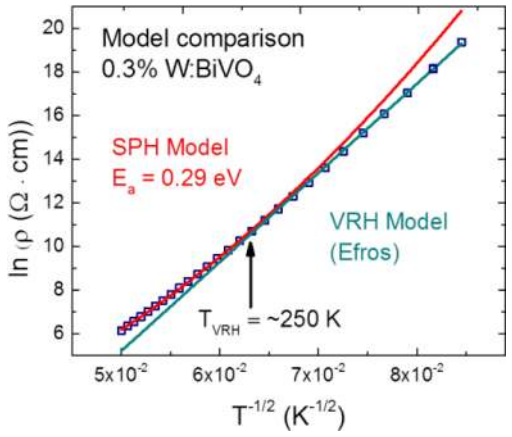

Figure 5. Fits of small polaron hopping (SPH) and variable range hopping (VRH) transport models to resistivity data. The arrow indicates the transition to the VRH mechanism.

Debye temperature ($\Theta_D/2$).[46] At the time of writing, no literature values for the Debye temperature of $BiVO_4$ exist, so on the basis of our data, we estimate a value of ~500 K.

In the VRH regime, conduction occurs by hopping from localized dopant centers and so can be applied in doped semiconductors and amorphous glasses containing metal ions. Several VRH mechanisms exist: Mott 3D, Mott 2D,[43] and Efros−Shkolvskii.[47] The Efros−Shkolvskii model gave the best fit to our data and is described by

$$\rho(T) \propto \exp\left(\frac{1}{T^{1/2}}\right) \tag{4}$$

though it should be noted that all models mentioned fit the data adequately ($R^2 > 0.999$). Interestingly, the relationship $\ln \rho \propto T^{-3/4}$ matched the resistivity data excellently over the entire temperature range (data not shown), but no conduction model was of this form. The data for 0.6% W:$BiVO_4$ crystals (Figure S5 of the SI) produced results nearly identical to those described above for 0.3% Mo:$BiVO_4$. Certainly, our understanding of transport in $BiVO_4$ would benefit from rigorous computational studies as have been performed for hematite[48,49] and titania.[50]

3.3.2. Resistivity Anisotropy. Monoclinic $BiVO_4$ (space group *I*2/*b*, a = 5.1935 Å, b = 5.0898 Å, c = 11.6972 Å, and γ = 90.387°)[22] has a layered structure, consisting of edge-sharing BiO_8 and VO_4 groups, separated by weakly bonded oxygen planes perpendicular to the *c* direction (Figure 6). Hoffart et al. investigated anisotropy in undoped single crystals at elevated temperatures (550−700 °C), where conduction is primarily

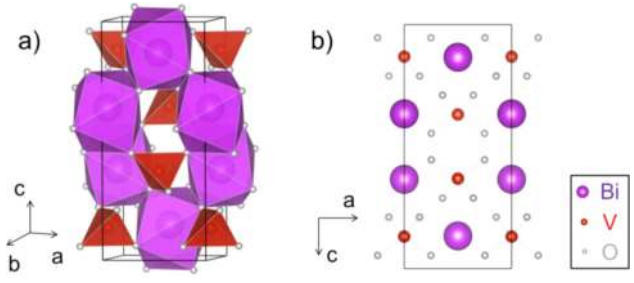

Figure 6. Schematic of monoclinic BiVO4 structure (a) showing edge-sharing BiO_8 (purple) and VO_4 (red) units and (b) illustrating oxygen planes perpendicular to the *c* direction.[57]

dx.doi.org/10.1021/ja405550k | J. Am. Chem. Soc. 2013, 135, 11389−11396

ionic and via oxygen vacancies.[23] The authors showed 50 times greater ionic resistivity in the *c* direction than in the *a* direction, which was attributed to the layered structure of $BiVO_4$. We measured a resistivity anisotropy ratio (ρ_c/ρ_{ab}) of ∼3 over multiple single-crystal samples at room temperature (Table 2),

Table 2. Resistivity Anisotropy of 0.3% W:$BiVO_4$ Single Crystals at 300 K

sample	geometry	technique	ρ_c/ρ_{ab}
1	*ab* plate	vdP[a]	2.6
2	*ab* plate	vdP[a]	3.7
3	bar	four-point collinear	2.9

[a]van der Pauw.

where $\rho_a \approx \rho_b = \rho_{ab}$ as discussed in section 3.3. This was first observed in the vdP geometry; however, direction-dependent resistivities could not be extracted using the traditional vdP method, which assumes that the sample is isotropic.[51] Several authors have presented techniques for determining resistivity anisotropy from vdP data.[52−55] Here, we have used Kazani et al.'s method,[56] which indicated an anisotropy ratio between 2.6 and 3.7.

To verify this result, bar-shaped samples (0.5 mm × 0.3 mm × 2 mm) were cut in the directions of interest and four-point collinear measurements confirmed an anisotropy ratio of ∼3 as shown in Table 2.

Though the degree of anisotropy is modest, this difference could be significant in $BiVO_4$-based photoelectrodes where charge transport is limiting. High-aspect ratio nanostructures that minimize electron transport in the *c* direction are therefore predicted to be beneficial in this case. Other recent work has emphasized the importance of crystal orientation in photoelectrochemical processes, such as, on different crystal facets of $BiVO_4$.[58]

The method of Kazani et al. was further tested by applying the technique to vdP data for *c* plates that were expected to be isotropic. This analysis yielded resistivities that varied by only 20−30% (Table S1 of the SI).

3.3.3. Hall Effect Measurements. We attempted to measure the Hall effect using a static magnetic field in the doped samples, but no clear signal above the instrument noise could be obtained. For these samples, it was noticed that it took several hours to reach a steady state after a current had been applied, and spurious Hall voltages could be easily obtained with an insufficient wait time. A potential explanation for the small signal is that the samples were too thick. The Hall voltage, V_H, is inversely proportional to sample thickness, *t*[59]

$$V_H = \frac{iB\rho\mu}{t} \tag{5}$$

where *i* is the applied current, *B* is the field strength, and μ is the mobility. Thin films (on the order of nanometers) would improve the Hall signal dramatically but also increase the misalignment voltage that is directly proportional to sample thickness.[32]

The ac field Hall effect measurements were used to obtain values for carrier mobility, μ, and carrier concentration, *n*, for the doped single crystals. This technique applies an oscillating magnetic field to the sample, making the resulting Hall voltage (given in eq 5) time-dependent. This signal is boosted by a lock-in amplifier, facilitating measurement of the Hall effect in low-mobility materials.[32] Though this is an uncommon technique, it is well established in the literature with work dating from the 1960s developing and utilizing it.[60,61] The ac field Hall effect measurements showed both W:$BiVO_4$ and Mo:$BiVO_4$ crystals were n-type with electron mobilities of ∼0.2 $cm^2\ V^{-1}\ s^{-1}$ at 300 K (Table S2 of the SI). In the temperature range of 250−300 K, mobility was effectively constant, while the carrier concentration decreased as the sample was cooled (Figure 7), consistent with the resistivity increase at lower

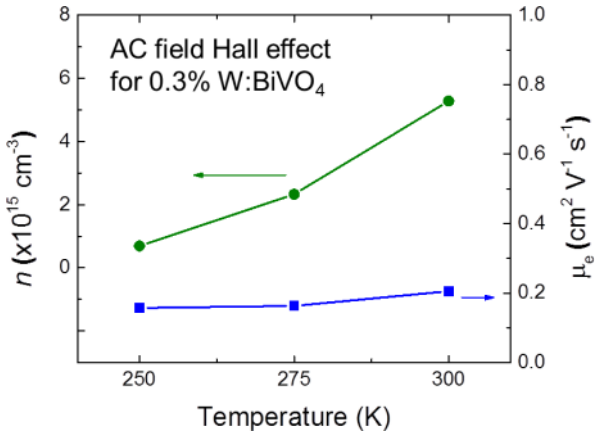

Figure 7. Carrier concentration (*n*) and electron mobility (μ_e) ac field Hall effect as a function of temperature for a 0.3% W:$BiVO_4$ *c* plate.

temperatures (Figure 4). Similar behavior was observed for 0.6% Mo:$BiVO_4$ (Figure S6 of the SI). Below 250 K, the signal was too noisy to discern a Hall voltage in the doped crystals and undoped samples were too resistive to measure the Hall effect at all temperatures considered. There was variability in the measurements (factor of ∼2) as the Hall voltage was small (Table S3 of the SI), but this did not appreciably change the observed trends or the values for *n* or μ_e. For an n-type semiconductor, the carrier concentration is given by

$$n = \frac{1}{\rho e \mu_e} \tag{6}$$

Using eq 6, *n* was determined to be ∼5×10^{15} cm^{-3} at 300 K (Table S2 of SI), significantly lower than the impurity concentrations, between 4 and 8 × 10^{19} cm^{-3} for 0.3% W and 0.6% Mo doping, respectively, calculated from ICP-MS measurements (Table 1). This unexpected result suggests partial charge compensation in these single crystals, which can complicate the intentional doping of complex metal oxides.[62] Under the O-rich and Bi-poor growth conditions employed, we hypothesize that singly ionized impurities substituted at the V site ($M_V^{\bullet}$) are the main sources of donors and triply charged Bi vacancies (V_{Bi}''') are the main sources of acceptors (eq 4), using Kröger−Vink notation:

$$n - p = [M_V^{\bullet}] - 3[V_{Bi}'''] \tag{7}$$

where *p* is the carrier concentration of holes, M is Mo or W, and the subscript refers to the lattice site. Bi vacancies have been observed in heavily doped (Mo and W) polycrystalline $BiVO_4$[12,29] and are predicted to be shallow acceptors that can easily be accommodated in the $BiVO_4$ lattice.[35,63] Unfortunately, the very low predicted concentration of these vacancies means they could not be observed in our lightly doped samples. From the charge balance in eq 9, it is clear that only a low concentration of Bi vacancies would be needed to provide a

dx.doi.org/10.1021/ja405550k | J. Am. Chem. Soc. 2013, 135, 11389−11396

significant degree of charge compensation. Addition of excess Bi in the feed rods may promote less compensation and more efficient n-type doping of $BiVO_4$;[62,64] however, a slight excess of V was required for stable growth of crystals experimentally.

3.4. Photoelectrochemistry. All photoelectrochemical testing was done with doped samples, as we could not obtain a measurable photocurrent from electrodes using undoped $BiVO_4$ crystals. This is attributed to recombination of generated electron−hole pairs before reaching the back contact, based on the inherently low conductivity of undoped crystals (Figure 4) and relatively large crystal thickness (~100 μm). Linear sweep voltammetry (LSV) was used to evaluate the performance of doped single-crystal $BiVO_4$ electrodes with the (001) face exposed, which exhibited behavior characteristic of an n-type photoanode (Figure 8a). Only Mo:$BiVO_4$ data are shown as the behavior of W:$BiVO_4$ electrodes was comparable (Figure S7 of the SI).

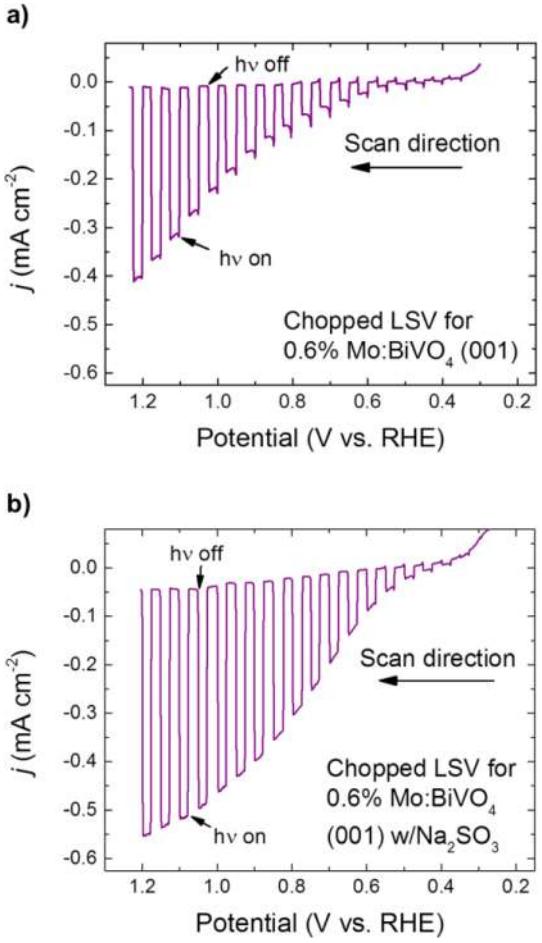

Figure 8. Chopped illumination linear sweep voltammograms (LSVs) of a Mo:$BiVO_4$ electrode with the (001) face exposed. The scan rate was 20 mV/s, and the light intensity was 100 mW/cm^2 from a xenon lamp. The electrolyte solution was 0.1 M phosphate buffer with (a) 0.1 M Na_2SO_4 or (b) 0.1 M Na_2SO_4, and 0.1 M Na_2SO_3 (hole scavenger).

Photocurrents reached ~0.4 mA/cm^2 at 1.2 V versus RHE (Figure 8a). A hole scavenger (Na_2SO_3) was used to evaluate electrode performance with facile oxidation kinetics (Figure 8b). Here, we observed the onset of the photocurrent at lower potentials than for water oxidation, demonstrating that the transfer of a hole from the $BiVO_4$ surface to the solution is limiting when it is used for water oxidation. This has been reported by other authors and illustrates the importance of cocatalysts for this material.[21,65,66] Relatively small cathodic dark currents were observed at more negative potentials (Figure 8a,b and Figure S7 of the SI) and may result from reduction of the electrode surface or dissolved oxygen in the electrolyte. Incident photon conversion efficiency (IPCE) spectra agreed well with polycrystalline $BiVO_4$ photoanodes with a tail extending to ~520 nm (Figure 9).[65,67] This indicates

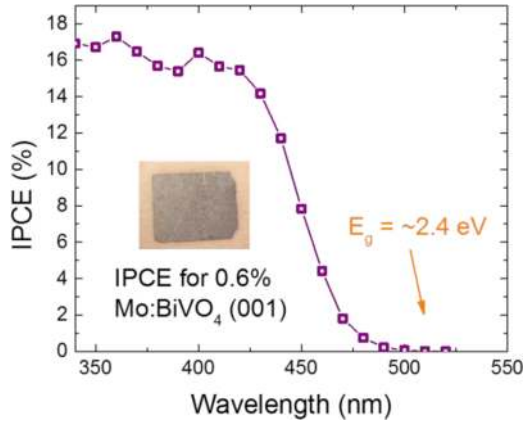

Figure 9. Incident photon to current efficiency at 1.2 V vs RHE in 0.1 M phosphate buffer with 0.1 M Na_2SO_4. The photograph of a Mo:$BiVO_4$ *c* plate (inset) shows the dark coloration of a doped single crystal.

a band gap (E_g of ~2.4 eV), despite the dark coloration of the doped single crystals (Figure 1). Diffuse reflectance UV−vis spectra showed that these samples absorb at all wavelengths of visible light (Figure S8 of the SI), but clearly these do not contribute to useful electron−hole generation. This phenomenon has been observed in reduced single-crystal TiO_2[68] and $SrTiO_3$,[69] doped ZnO,[70] and, most recently, H_2-treated polycrystalline $BiVO_4$ films,[63] but the underlying mechanism remains unclear. Future work will involve photoluminescence measurements to probe the role of impurity states and carrier recombination in our crystals.

3.4.1. Mott−Schottky Analysis. Mott−Schottky (M−S) analysis is commonly used in photoelectrode characterization and relies on measuring the capacitance of the space charge region at the semiconductor−liquid junction. The flat band potential, V_{fb}, is determined from a plot of C_{SC}^{-2} versus potential as the *x* intercept and the carrier concentration can be calculated using the slope of the linear region according to eq 8 for an n-type semiconductor

$$\frac{1}{C_{SC}^{\ 2}} = \left(\frac{2}{\varepsilon\varepsilon_0 en}\right)\left(V - V_{fb} - \frac{k_B T}{e}\right) \quad (8)$$

where ε is the dielectric constant of the material, ε_0 is the permittivity of free space, and V is the applied potential. The term k_BT/e is small at room temperature and therefore neglected.

Both the calculated flat band potential and carrier concentrations were shown to vary with frequency (Figure S9 of the SI). The flat band potential was 0.03−0.08 V versus RHE, in good agreement with the onset potential of ~0.05 V (Figure S7, inset, of the SI). The calculated range of carrier concentration from these plots was 0.3 to 1 × 10^{18} cm^{-3}. This

dx.doi.org/10.1021/ja405550k | J. Am. Chem. Soc. 2013, 135, 11389−11396

value does not agree with n from Hall effect measurements and illustrates the need for independent measurement of this quantity. The frequency dispersion indicates that M−S analysis may not be adequate for accurate determinations of n for these single crystals. This finding has also been observed for other single-crystal electrodes, such as hematite.[69]

3.4.2. Estimation of Hole Diffusion Length. Via application of the model of Gärtner,[71] a useful relationship can be derived for estimating the hole diffusion length:[72,73]

$$\ln(1-\eta) = -\alpha\left(\frac{\varepsilon\varepsilon_0}{2en}\right)^{1/2}(V - V_{fb})^{1/2} - \ln(1 + \alpha L_p) \quad (9)$$

where η is the IPCE in eq 2 corrected for reflection at the electrode surface and expressed as a fraction, α is the absorption coefficient, and L_p is the minority carrier diffusion length. At sufficiently positive potentials, a plot of $\ln(1-\eta)$ versus $(V - V_{fb})^{1/2}$ results in a linear region that can be extrapolated to the y intercept to determine L_p (Figure S10 of the SI). Application of this analysis yielded a value for α of ∼2,600 cm^{-1} using n from the ac Hall effect measurements and a resulting hole diffusion length of ∼100 nm at λ = 400 nm. This value is in agreement with the estimated range of 100−200 nm calculated by other authors for polycrystalline undoped and doped $BiVO_4$ electrodes.[18] Detailed calculations are given in the SI.

3.5. Comparison to Other Metal Oxide Photoanode Materials. The electron mobility of Mo:$BiVO_4$ and W:$BiVO_4$ is low, but in the correct range for metal oxide semiconductors in which thermally activated small polaron hopping is the dominant conduction mechanism. In comparison to those of other metal oxides studied as photoanodes, its intrinsic mobility is on the low side, similar to that of iron oxide (Table S4 of the SI). However, the hole diffusion length is moderate, being greater than reported values for single-crystal TiO_2 and polycrystalline hematite (at the time of writing, no single-crystal data for comparison could be found), but significantly less than that of monoclinic WO_3 (Table S5 of the SI).

It is important to note that mobility is a function of total impurity concentration because of scattering processes, and although the n of these single crystals was low because of charge compensation, the impurity concentration was on the order of 10^{19} cm^{-3} (calculated on the basis of ICP-MS measurements). If fewer of the donor impurities were compensated, samples with lower resistivity and lower impurity concentrations could be synthesized, potentially resulting in higher electron mobility because of reduced impurity scattering. Further studies of doping on grain boundaries and surface states as has been performed for other materials[74,75] are essential to an in-depth understanding of this material and optimization of $BiVO_4$ for water splitting applications.

4. CONCLUSIONS

We have synthesized single crystals of undoped $BiVO_4$, Mo:$BiVO_4$, and W:$BiVO_4$ via the floating zone technique, with up to 0.6 and 0.3% doping, respectively. Mo and W substitute for V in $BiVO_4$ and act as donor impurities, doping crystals of the n type. Between 250 and 400 K, conduction is governed by small polarons, with an associated activation energy of 0.3 eV. At temperatures lower than 250 K, a transition to a variable-range hopping mechanism occurs. A resistivity anisotropy of ∼3 was observed in the c direction and was attributed to the layered structure of $BiVO_4$. Attempts to measure the dc field Hall effect were unsuccessful, but the ac field technique yielded an electron mobility of ∼0.2 $cm^2\ V^{-1}\ s^{-1}$ at 300 K. Comparison of the impurity level to the carrier concentration indicated partial charge compensation in these crystals. Mott−Schottky analysis yielded a flat band potential of 0.03−0.08 V versus RHE, while IPCE tests showed that the dark coloration of the doped single crystals did not contribute to additional photocurrent. Applying the Gärtner model, we estimated a hole diffusion length of ∼100 nm. These results provide new insights into the fundamental transport properties of $BiVO_4$ and should be of great value in optimizing this material further for photoelectrochemistry and other applications.

■ ASSOCIATED CONTENT

Supporting Information

Detailed experimental procedures, transflectance data, additional resistivity, ac Hall and PEC data, Mott−Schottky analysis, hole diffusion length calculations, and tabulated mobilities and hole diffusion lengths from the literature. This material is available free of charge via the Internet at http://pubs.acs.org.

■ AUTHOR INFORMATION

Corresponding Author

mullins@che.utexas.edu

Notes

The authors declare no competing financial interest.

■ ACKNOWLEDGMENTS

We gratefully acknowledge the U.S. Department of Energy (DOE) Grant DE-FG02-09ER16119 and the Welch Foundation (Grants F-1436 to C.B.M. and F-0021 to A.J.B.). Resistivity and dc Hall effect measurements were taken in the Environmental Molecular Sciences Laboratory, a national scientific user facility sponsored by the Office of Biological and Environmental Research of the DOE and located at Pacific Northwest National Laboratory. We are indebted to T. C. Droubay and S. A. Chambers for their help with the PPMS. Additionally, A.J.E.R. thanks W. D. Chemelewski for help with anisotropic vdP data analysis and useful discussions as well as the Thrust 2000 Graduate Fellowship in Engineering (Harry P. Whitworth endowed and Wayne Nance Family endowed). J.-F.L. was supported as part of EFree, an Energy Frontier Research Center funded by the DOE Office of Science, Office of Basic Energy Sciences, under Award DE-SC0001057. We gratefully acknowledge C. J. Stolle and B. A. Korgel for their help with diffuse reflectance UV−vis spectroscopy measurements.

■ REFERENCES

(1) Bard, A. J.; Fox, M. A. *Acc. Chem. Res.* **1995**, *28*, 141.
(2) Grätzel, M. *Nature* **2001**, *414*, 338.
(3) Ni, M.; Leung, M. K.; Leung, D. Y.; Sumathy, K. *Renewable Sustainable Energy Rev.* **2007**, *11*, 401.
(4) Sivula, K.; Le Formal, F.; Grätzel, M. *ChemSusChem* **2011**, *4*, 432.
(5) Liu, X.; Wang, F.; Wang, Q. *Phys. Chem. Chem. Phys.* **2012**, *14*, 7894.
(6) Park, Y.; McDonald, K. J.; Choi, K.-S. *Chem. Soc. Rev.* **2013**, *42*, 2321.
(7) Li, Z.; Luo, W.; Zhang, M.; Feng, J.; Zou, Z. *Energy Environ. Sci.* **2013**, *6*, 347.

(8) Berglund, S. P.; Flaherty, D. W.; Hahn, N. T.; Bard, A. J.; Mullins, C. B. *J. Phys. Chem. C* **2011**, *115*, 3794.
(9) Tokunaga, S.; Kato, H.; Kudo, A. *Chem. Mater.* **2001**, *13*, 4624.
(10) Bierlein, J. D.; Sleight, A. W. *Solid State Commun.* **1975**, *16*, 69.
(11) Pinczuk, A.; Welber, B.; Dacol, F. *Solid State Commun.* **1979**, *29*, 515.
(12) Sleight, A. W.; Aykan, K.; Rogers, D. B. *J. Solid State Chem.* **1975**, *13*, 231.
(13) Pilli, S. K.; Furtak, T. E.; Brown, L. D.; Deutsch, T. G.; Turner, J. A.; Herring, A. M. *Energy Environ. Sci.* **2011**, *4*, 5028.
(14) Luo, W.; Yang, Z.; Li, Z.; Zhang, J.; Liu, J.; Zhao, Z.; Wang, Z.; Yan, S.; Yu, T.; Zou, Z. *Energy Environ. Sci.* **2011**, *4*, 4046.
(15) Luo, W.; Wang, J.; Zhao, X.; Zhao, Z.; Li, Z.; Zou, Z. *Phys. Chem. Chem. Phys.* **2013**, *15*, 1006.
(16) Luo, W.; Li, Z.; Yu, T.; Zou, Z. *J. Phys. Chem. C* **2012**, *116*, 5076.
(17) Ye, H.; Park, H. S.; Bard, A. J. *J. Phys. Chem. C* **2011**, *115*, 12464.
(18) Zhong, D. K.; Choi, S.; Gamelin, D. R. *J. Am. Chem. Soc.* **2011**, *133*, 18370.
(19) Abdi, F. F.; Firet, N.; van de Krol, R. *ChemCatChem* **2013**, *5*, 490.
(20) Park, H. S.; Kweon, K. E.; Ye, H.; Paek, E.; Hwang, G. S.; Bard, A. J. *J. Phys. Chem. C* **2011**, *115*, 17870.
(21) Berglund, S. P.; Rettie, A. J. E.; Hoang, S.; Mullins, C. B. *Phys. Chem. Chem. Phys.* **2012**, *14*, 7065.
(22) Sleight, A. W.; Chen, H. Y.; Ferretti, A.; Cox, D. E. *Mater. Res. Bull.* **1979**, *14*, 1571.
(23) Hoffart, L.; Heider, U.; Huggins, R. A.; Witschel, W.; Jooss, R.; Lentz, A. *Ionics* **1996**, *2*, 34.
(24) Hoffart, L.; Heider, U.; Joerissen, L.; Huggins, R. A.; Witschel, W. *Solid State Ionics* **1994**, *72*, 195.
(25) Hoffart, L.; Heider, U.; Jorissen, L.; Huggins, R. A.; Witschel, W. *Ionics* **1995**, *1*, 131.
(26) Hartmanova, M.; Le, M. T.; Jergel, M.; Smatko, V.; Kundracik, F. *Russ. J. Electrochem.* **2009**, *45*, 621.
(27) Beg, S.; Haneef, S.; Al-Areqi, N. A. S. *Phase Transitions* **2010**, *83*, 1114.
(28) Vinke, I. C.; Diepgrond, J.; Boukamp, B. A.; De, V. K. J.; Burggraaf, A. J. *Solid State Ionics* **1992**, *57*, 83.
(29) Cesari, M.; Perego, G.; Zazzetta, A.; Manara, G.; Notari, B. *J. Inorg. Nucl. Chem.* **1971**, *33*, 3595.
(30) McCloy, J. S.; Ryan, J. V.; Droubay, T.; Kaspar, T. C.; Chambers, S.; Look, D. C. *Rev. Sci. Instrum.* **2010**, *81*, 063902.
(31) Look, D. C. *Electrical characterization of GaAs materials and devices*; Wiley: New York, 1989.
(32) Lindemuth, J.; Mizuta, S.-I. In *SPIE Solar Energy + Technology*; International Society for Optics and Photonics: Bellingham, WA, 2011; p 81100I.
(33) Chen, Z.; Jaramillo, T. F.; Deutsch, T. G.; Kleiman-Shwarsctein, A.; Forman, A. J.; Gaillard, N.; Garland, R.; Takanabe, K.; Heske, C.; Sunkara, M. *J. Mater. Res.* **2010**, *25*, 3.
(34) Nassu, K. *Am. Mineral.* **1978**, *63*, 219.
(35) Yin, W.-J.; Wei, S.-H.; Al-Jassim, M. M.; Turner, J.; Yan, Y. *Phys. Rev. B* **2011**, *83*, 155102.
(36) Klein, C.; Hurlbut, C. S.; Dana, J. D. *Manual of mineralogy*; Wiley: New York, 1993; Vol. *527*.
(37) Koohpayeh, S.; Fort, D.; Abell, J. *Prog. Cryst. Growth Charact. Mater.* **2008**, *54*, 121.
(38) Frost, R. L.; Henry, D. A.; Weier, M. L.; Martens, W. *J. Raman Spectrosc.* **2006**, *37*, 722.
(39) Zhang, H. M.; Liu, J. B.; Wang, H.; Zhang, W. X.; Yan, H. *J. Nanopart. Res.* **2008**, *10*, 767.
(40) Bosman, A.; Van Daal, H. *Adv. Phys.* **1970**, *19*, 1.
(41) Zhao, B.; Kaspar, T. C.; Droubay, T. C.; McCloy, J.; Bowden, M. E.; Shutthanandan, V.; Heald, S. M.; Chambers, S. A. *Phys. Rev. B: Condens. Matter Mater. Phys.* **2011**, *84*, 245325/1.
(42) Yildiz, A.; Lisesivdin, S.; Kasap, M.; Mardare, D. *Phys. B (Amsterdam, Neth.)* **2009**, *404*, 1423.
(43) Mott, N. F.; Davis, E. A. *Electronic processes in non-crystalline materials*, 2nd ed.; OUP: Oxford, U.K., 1979.
(44) Emin, D.; Seager, C.; Quinn, R. K. *Phys. Rev. Lett.* **1972**, *28*, 813.
(45) Austin, I. G.; Mott, N. F. *Adv. Phys.* **1969**, *18*, 41.
(46) Holstein, T. *Ann. Phys.* **1959**, *8*, 343.
(47) Efros, A.; Shklovskii, B. *J. Phys. C Solid State Phys.* **1975**, *8*, L49.
(48) Rosso, K. M.; Smith, D. M.; Dupuis, M. *J. Chem. Phys.* **2003**, *118*, 6455.
(49) Iordanova, N.; Dupuis, M.; Rosso, K. M. *J. Chem. Phys.* **2005**, *122*, 144305.
(50) Deskins, N. A.; Dupuis, M. *Phys. Rev. B* **2007**, *75*, 195212.
(51) Van der Pauw, L. *Philips Tech. Rev.* **1958**, *20*, 220.
(52) Price, W. *J. Phys. D: Appl. Phys.* **2002**, *5*, 1127.
(53) Bierwagen, O.; Pomraenke, R.; Eilers, S.; Masselink, W. *Phys. Rev. B* **2004**, *70*, 165307.
(54) Montgomery, H. *J. Appl. Phys.* **1971**, *42*, 2971.
(55) dos Santos, C. A. M.; de Campos, A.; da Luz, M. S.; White, B. D.; Neumeier, J. J.; de Lima, B. S.; Shigue, C. Y. *J. Appl. Phys.* **2011**, *110*, 083703.
(56) Kazani, I.; De Mey, G.; Hertleer, C.; Banaszczyk, J.; Schwarz, A.; Guxho, G.; Van Langenhove, L. *Text. Res. J.* **2011**, *81*, 2117.
(57) Momma, K.; Izumi, F. *J. Appl. Crystallogr.* **2011**, *44*, 1272.
(58) Li, R.; Zhang, F.; Wang, D.; Yang, J.; Li, M.; Zhu, J.; Zhou, X.; Han, H.; Li, C. *Nat. Commun.* **2013**, *4*, 1432.
(59) Streetman, B. G.; Banerjee, S. *Solid state electronic devices*, 6th ed.; Prentice Hall: Upper Saddle River, NJ, 2006.
(60) Hermann, A.; Ham, J. *Rev. Sci. Instrum.* **1965**, *36*, 1553.
(61) Parker, D.; Yahia, J. *Phys. Rev.* **1968**, *169*, 605.
(62) van de Krol, R., Grätzel, M., Eds. *Photoelectrochemical Hydrogen Production*; Springer: Berlin, 2012.
(63) Wang, G.; Ling, Y.; Lu, X.; Qian, F.; Tong, Y.; Zhang, J. Z.; Lordi, V.; Rocha Leao, C.; Li, Y. *J. Phys. Chem. C* **2013**, *117*, 10957.
(64) Abdi, F. F.; Firet, N.; van de Krol, R. *ChemCatChem* **2013**, *5*, 490.
(65) Seabold, J. A.; Choi, K.-S. *J. Am. Chem. Soc.* **2012**, *134*, 2186.
(66) Abdi, F. F.; van de Krol, R. *J. Phys. Chem. C* **2012**, *116*, 9398.
(67) Liang, Y.; Tsubota, T.; Mooij, L. P.; van de Krol, R. *J. Phys. Chem. C* **2011**, *115*, 17594.
(68) Kavan, L.; Grätzel, M.; Gilbert, S. E.; Klemenz, C.; Scheel, H. J. *J. Am. Chem. Soc.* **1996**, *118*, 6716.
(69) Finklea, H. O. *Semiconductor electrodes*; Elsevier Science Ltd.: Amsterdam, 1988.
(70) Paulauskas, I. E.; Jellison, G. E.; Boatner, L. A.; Brown, G. M. *Int. J. Electrochem.* **2011**, *2011*.
(71) Gärtner, W. W. *Phys. Rev.* **1959**, *116*, 84.
(72) Kennedy, J. H.; Frese, K. W. *J. Electrochem. Soc.* **1976**, *123*, 1683.
(73) Kennedy, J. H.; Frese, K. W. *J. Electrochem. Soc.* **1978**, *125*, 709.
(74) Chen, Z.; Forman, A. J.; Jaramillo, T. F. *J. Phys. Chem. C* **2013**, *117*, 9713.
(75) Frank, S. N.; Bard, A. J. *J. Am. Chem. Soc.* **1975**, *97*, 7427.